ADVANCED MATERIALS
www.advmat.de

# When Chirophotonic Film Meets Wrinkles: Viewing Angle Independent Corrugated Photonic Crystal Paper

*Seok-In Lim, Eunji Jang, Dongmin Yu, Jahyeon Koo, Dong-Gue Kang, Kyung Min Lee, Nicholas P. Godman, Michael E. McConney, Dae-Yoon Kim,* and Kwang-Un Jeong**

**Light manipulation strategies of nature have fascinated humans for centuries. In particular, structural colors are of considerable interest due to their ability to control the interaction between light and matter. Here, wrinkled photonic crystal papers (PCPs) are fabricated to demonstrate the consistent reflection of colors regardless of viewing angles. The nanoscale molecular self-assembly of a cholesteric liquid crystal (CLC) with a microscale corrugated surface is combined. Fully polymerizable CLC paints are uniaxially coated onto a wrinkled interpenetrating polymer network (IPN) substrate. Photopolymerization of the helicoidal nanostructures results in a flexible and free-standing PCP. The facile method of fabricating the wrinkled PCPs provides a scalable route for the development of novel chirophotonic materials with precisely controlled helical pitch and curvature dimensions. The reflection notch position of the flat PCP shifts to a lower wavelength when the viewing angle increased, while the selective reflection wavelength of wrinkled PCP is remained consistent regardless of viewing angles. The optical reflection of the 1D stripe-wrinkled PCP is dependent on the wrinkle direction. PCPs with different corrugated directions can be patterned to reduce the angular-dependent optical reflection of wrinkles. Furthermore, 2D wavy-wrinkled PCP is successfully developed that exhibit directionally independent reflection of color.**

## 1. Introduction

Rod-shaped molecules with molecular chirality can form a spontaneous helical nanostructure with a twist axis perpendicular to the local director, resulting in the formation of a cholesteric liquid crystal (CLC) phase.[1] The most striking features of the CLC phase are its exceptional optical rotatory power and structural colors due to the selective reflection of light.[2] Structural colors are the result of light interference phenomena, such as Bragg reflection caused by periodic nanostructures and the average refractive index of rod-shape molecules. The initial notch position of CLC can be expressed by the equation $\lambda_0 = n \times P_0$, where $\lambda_0$ is the initial notch position, $n$ is the average refractive index, and $P_0$ is the initial pitch length.[3] Nature has adopted this helical nanostructure to provide various color information to the epidermis of petals, butterfly wings, and the cuticle of beetles.[4] Inspired by such natural photonic nanostructures, a number of researchers fabricate artificial structural colors using photonic crystals, plasmonic nanostructures, and metamaterials.[5] These examples of natural helical nanostructures and studies of artificial structural colors have been used to design materials with advanced functionalities, such as those used in optical sensing, camouflage, and anti-counterfeiting technology.[6]

However, most artificial structural color materials are angular dependent and are of limited use in display devices, print media, and optical sensing as they require wide viewing angles.[7] Many living organisms in nature have low-angle-dependent or angle-independent structural colors that are used for warnings, displays, or conspecific communications.[8] To overcome the angle-dependent limitations of artificial structural color materials, researchers once again looked for answers in nature and found that organisms such as some mammals and insects exhibit low-angle-dependent or angle-independent structural colors via amorphous colloidal arrays.[9] For example, blue color in mandrills' cheeks is due to parallel dermal collagen fibers formed in a short-range order.[10] Monodispersed chitinous particles in the epidermal cells of dragonflies also display an angular-independent blue color.[11] Nature produces colloidal arrays with controlled nanostructures, and regulates the microstructure of the surface that display the angular independent colors. The most prevalent example of structurally enhanced color and iridescence are found in petals, which are composed of periodically wrinkled epidermal cells that act as

S.-I. Lim, E. Jang, D. Yu, J. Koo, K.-U. Jeong
Department of Polymer-Nano Science and Technology
Department of Nano Convergence Engineering
Jeonbuk National University
Jeonju 54896, Republic of Korea
E-mail: kujeong@jbnu.ac.kr

D.-G. Kang, D.-Y. Kim
Functional Composite Materials Research Center
Korea Institute of Science and Technology
Wanju 55324, Republic of Korea
E-mail: kdaeyoon@kist.re.kr

K. M. Lee, N. P. Godman, M. E. McConney
US Air Force Research Laboratory Wright-Patterson Air Force Base
Dayton, Ohio 45433, USA

The ORCID identification number(s) for the author(s) of this article can be found under https://doi.org/10.1002/adma.202206764.

**DOI: 10.1002/adma.202206764**

 

diffractive gratings.[12] Thus, there has been a growing interest in a thorough understanding and mimicking of the natural colors' optical properties and the complex correlation between nano- and micro-structures to overcome the angular-dependent limitations of artificial structural colors.

In recent years, surface wrinkling has been widely applied in a number of fields, and is used to control the surface wettability, dynamic optical properties, and flexibility of electronic devices.[13] Generally, wrinkles form due to accumulated compressive strain on a material, which can be caused by heating, solvent swelling, mechanical stretching, or crosslinking of gels.[14] Among them, mechanical stretching is commonly used to produce a wrinkled structure with easily adjustable crest and valley dimensions. When mechanical stretching stress exceeds a certain value, a compressive strain occurs on the surface of the material, which leads to the formation of wrinkles.[15] Due to the unique morphology of wrinkles, they are regarded as a type of smart surface that can be applied in optical elements. Indeed, wrinkled surfaces are characterized by structural irregularities, which make them effective over a wide spectral and angular range with respect to periodic diffraction gratings.[16] For example, Zhang et al. reported that bending-induced surface wrinkles can be used as an optical diffuser and can enhance light harvesting effectiveness.[17] Gao et al. developed a self-wrinkling polymer surface that utilized encapsulation of light emitting diode to improve light diffraction efficiency.[18] The unique properties of controlled wrinkled surfaces can enable the design of important optical materials that cannot be produced using conventional flat materials.

Herein, we report the development of 1D stripe and 2D wavy wrinkled photonic crystal papers that possess excellent viewing angle independent reflection of color. Coatable photonic crystal materials were prepared by molecular self-assembly of nematic and chiral reactive mesogens (RMs). CLC paints were uniformly shear coated on wrinkled interpenetrating polymer network (IPN) rubber substrates. The silicone rubber (SR) layer was automatically wrinkled on the acrylic rubber (AR) surface after the cured elastomers were relaxed under a certain deformation. The pre-strain was adjusted to generate 1D stripe- and 2D wavy-patterned wrinkles on the IPN substrate. Surface replication of the IPN substrate made it possible to construct photonic crystal paper (PCP) with a novel wrinkled structure following in situ photopolymerization of the CLC layer to fix its helical nanostructure and microscale topography.[19] The 1D stripe-wrinkled PCP demonstrated angular-independent reflection of color. In addition, the 2D wavy-wrinkled PCP exhibited directional independence of reflection color and both materials can be applied as an anti-counterfeiting film and a wide-angle monochromatic light reflector.

## 2. Results and Discussion

### 2.1. Fabrication of Wrinkled Chirophotonic Crystal Paper

A eutectic and homogeneous mixtures of cholesteric liquid crystal (CLC) paints are used to fabricate viewing angle independent photonic crystal papers (PCPs) by applying the shear coating process with CLC paints at room temperature. A chiral dopant with a photopolymerizable group (BPcRM) is a core component of the CLC paints, as shown in **Figure 1**a, and the synthetic method is described in our previous paper.[20] Since crystallization of the nematic host can interfere with the reliable coatability, two types of diacrylate-based reactive mesogen (RM257 and LC242) are used concurrently in this study. Notably, RM257 and LC242 itself show the crystalline state at room temperature. When RM257 and LC242 are mixed in a weight ratio of 1:1, the noticeable phase separation behaviors are not found for several hours by forming eutectic mixtures.[21] Thus, the CLC paints composed of BPcRM, RM257, and LC242 maintain their ordered structure without phase separation, resulting in significantly improved processability even at room temperature. The viscoelasticity of the CLC paint prepared from the eutectic mixtures is appropriate for shear coating on various geometry of substrates. We can demonstrate the wrinkled PCP through in situ photo-polymerization by uniaxially coating the wrinkled substrates with CLC paint to transfer the information of the wavy-like structures in the micrometer scale as well as the helical structures in the nanometer level (Figure 1b).

The fabrication of the wrinkled substrate is schematically illustrated in Figure S1 (Supporting Information). In the first stage of the pre-stretching process, we developed an interpenetrating polymer network (IPN) based on acrylic rubber (AR) and silicone rubber (SR). As IPNs composed of AR and SR have low mixing entropy, two distinct polymers are mixed with each other, which increases the continuity of the components at the molecular scale forming a stable IPN.[22] Thus, it is possible to create a desired wrinkle scale as well as freely make 1D stripe and 2D wavy wrinkled by adjusting the pre-strain of the IPN substrate. AR film is immersed in an oligomer solution of SR in *n*-heptane solvent. After reaching the equilibrium swelling state, the swollen AR film wrapped with SR (AR/SR) is dried at room temperature to remove the solvent. The dried AR/SR substrates are uniaxially stretched for 100%, and subsequently cured for 1 h at 100 °C. After releasing process, the optical microphotograph (OM with reflection mode of 100% IPN substrate exhibited sinusoidal stripe wrinkles on its surface along the pre-strain direction (Figure 1c). Note that the 0% IPN substrate is referred as a flat substrate prepared without the stretching and releasing steps.

To compare the influence of surface topography, the CLC paints are coated onto the 0% and 100% IPN substrate, and then polymerized to stabilize the helical nanostructures. After peeling off the 0% and 100% IPN substrate, we obtain the free-standing flat and wrinkled PCP, respectively (inset of Figure 1d,e). We can uniformly align the self-assembled CLC nanostructure on the IPN substrates by simple shear coating.[23] The helical axis (HA) of the hierarchical nanostructure is uniformly aligned parallel to the normal direction of the IPN surface so that the brilliant selective green light is reflected, as shown in Figure 1d,e. While the randomly distributed HA results in discontinuities in refractive index between the CLC domains, the flat and wrinkled PCP in the focal conic state scatters the light (Figure S2, Supporting Information).[24] For flat PCP, the planar textures developed evenly over the entire region. Importantly, the chiral nematic phase remains intact after polymer stabilization, indicating that the *R*-configured chirality of BPcRM at the molecular level is successfully

 

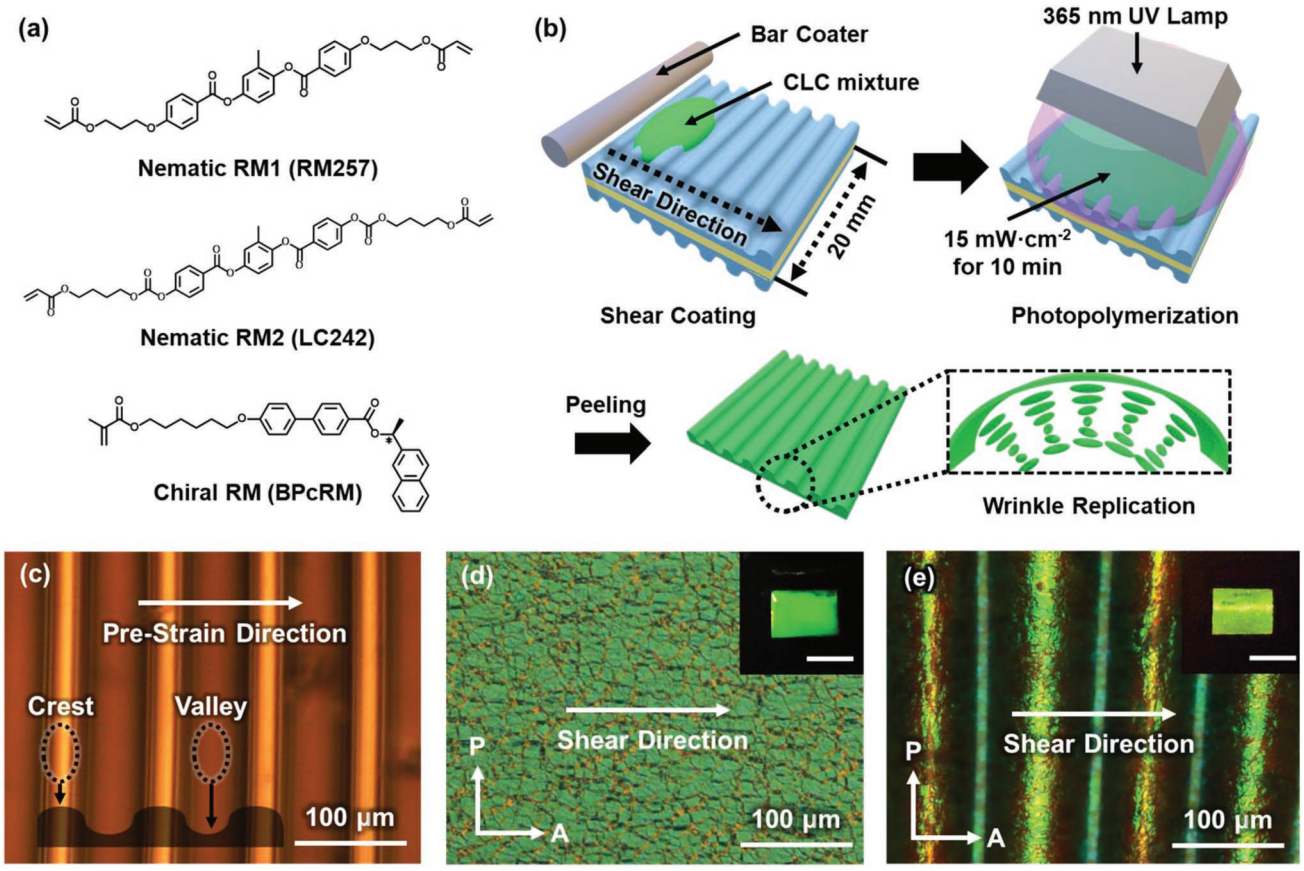


**Figure 1.** a) Chemical structures of the chiral and achiral RMs used to construct the helical nanostructures and b) schematic procedure of a wrinkle replication method to fabricate free-standing photonic crystal paper by using wrinkled IPN rubber as the substrate. c) OM image of the wrinkled IPN substrate with reflection mode. POM image of d) the flat PCP and e) the wrinkled PCP. Scale bar in the inset image is 10 mm.

transferred to the phase level. The wrinkled PCP also shows the planar textures with alternating green-dark-green stripes attributed to the repetitive crest-slope-valley region, which means that the CLC domain is uniaxially oriented even in the wavy surfaces.

Since the notch position of the PCP was determined by the helical pitch, the three different CLC paints were prepared by considering the helical twisting power. The optical microphotographs (OM) with reflection mode indicate that the CLC paints consisted with 8, 10, and 12 wt% BPcRM produce the wrinkled PCPs showing the selective reflection of red, green, and blue colors, respectively (**Figure 2**a–c). Because the shear direction (SD) is parallel to the wrinkle direction (WD), the helical nanostructure forms along the crests and valleys. As shown in Figure 2d, we measure the red, green, and blue color from the flat and wrinkled PCP according to viewing position. Here, the observer direction (OD) is parallel to the WD, and viewing angle ($\theta$) is tilted away from the film normal direction. When the structural colors are observed at $\theta = 3°$, the flat and wrinkled PCPs reflect red, green, and blue. Interestingly, the flat and wrinkled PCP showed not only the selective reflection of RGB colors, but also the circular polarization of light because the chirality governs the helicity of the nanostructures. The flat and wrinkled PCP showed its reflection colors when probed with right-handed circularly polarized light. Any reflection color is not observed when the left-handed circularly polarized light was illuminated (Figure 2e), and this chiroptical property is characterized in Figure 2f. The initial red, green, and blue reflection of flat PCP at $\theta = 3°$ is changed to green, blue, and colorless at $\theta = 60°$, while the wrinkled PCP maintains its original structural colors.

To systematically quantify the light reflection of the wrinkled PCP, reflection beams are projected onto a translucent hemispherical dome screen made of a white ping-pong ball (**Figure 3**a,b). The flat and wrinkled PCPs are placed underneath the center of the dome, and collimated white light passes through the pinhole at different angles ($\theta = 30°$ and 60°).[25] At $\theta = 30°$, the circular screen reveals the uniform greenish color selectively reflected from the flat PCP surface (Figure 3c). When the incident angle of light reaches 60°, the position of the reflected light shifts to the opposite side of the light source, and the color circle dramatically turns bluish indicating that the reflection color by the flat PCP is strongly affected by the viewing angle (Figure 3d). However, when using the wrinkled PCP, color dots of the same size as the incident light spot are observed, and color strip extending up and down occurs due to the unique reflective properties of the wrinkled PCP (Figure 3e,f). The translucent hemispherical dome screen observation with wrinkled PCP indicates the fact that the reflection color at $\theta = 30°$ and 60° is almost identical, unlike the flat PCP.

 

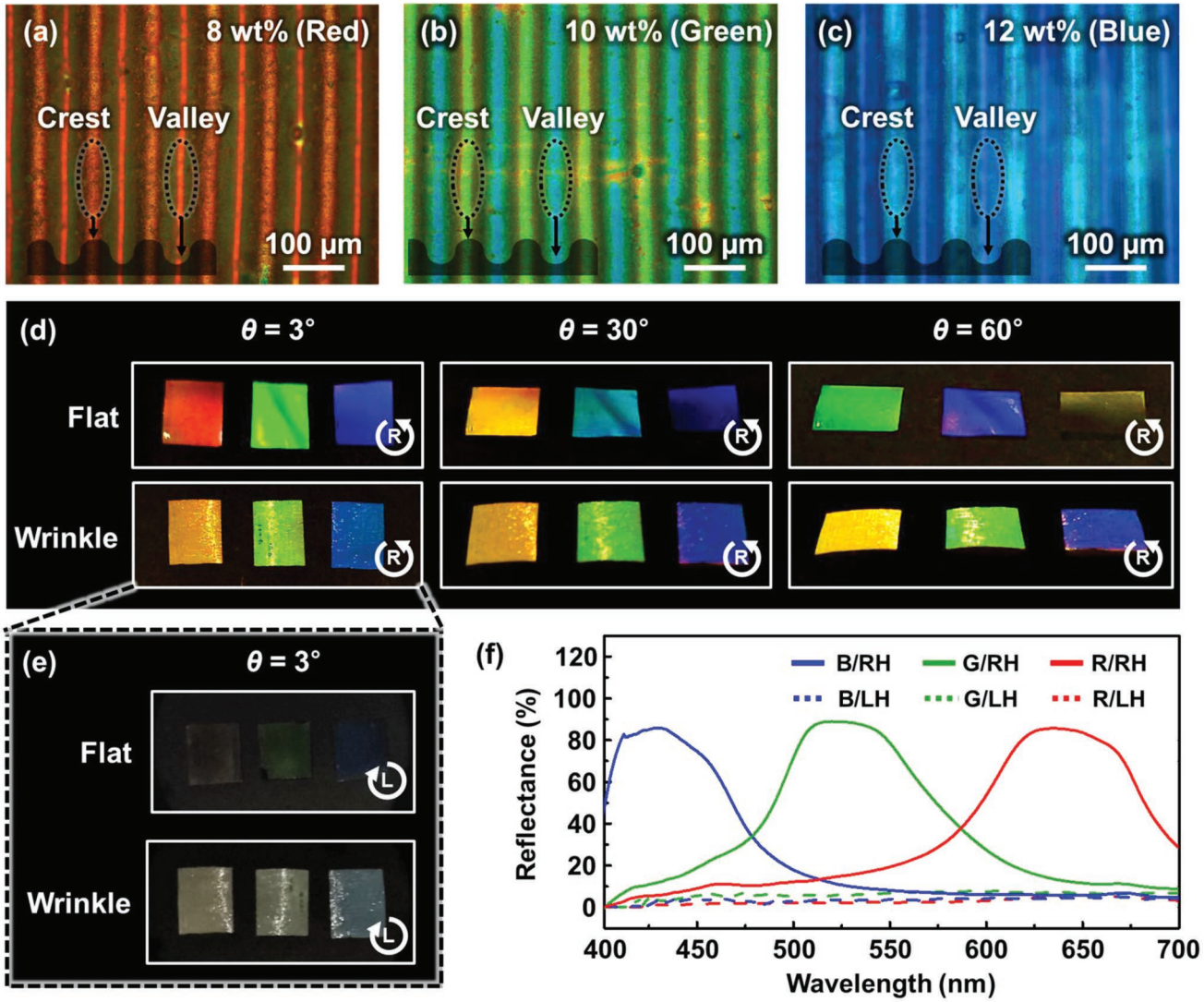


**Figure 2.** OM images with reflection mode of the wrinkled PCP obtained from the CLC mixture doped with a) 8, b) 10, and c) 12 wt% BPcRM. d) Macroscopic images of flat and wrinkled PCP observed at different viewing angles. Here, PCP is viewed under a right-handed circular polarizer. e) The reflection color for both flat and wrinkled PCP is mostly lost when probed with a left-handed circular polarizer. f) Reflectance spectra of the PCP probed with left- or right-handed circularly polarized light.

The transmittance and reflectance spectra of the flat and wrinkled PCP were measured to analyze their angular independence. Basically, the absorption wavelength region of CLC paint is located at 250 nm owing to the benzoate function in the molecular level (Figure S3, Supporting Information). In addition, human eyes can only detect the wavelength in the visible region between 400 and 800 nm. Therefore, transmission and reflection characteristics in the UV and IR regions were not considered. As shown in Figure S4 (Supporting Information), the 43% and 35% peak in reflection arise from the flat and wrinkled PCP, respectively. Since the macroscopic dimension of the flat PCP at $\theta = 3°$ is higher than the wrinkled PCP due to the slope region between the crest and valley, the reflection intensity of the wrinkled PCP is lower than the flat PCP. The sum of transmittance and reflectance is ≈91% and 73% for flat and wrinkled PCP, respectively. These results are also well matched with the translucent hemispherical screen experiments. The sharp and broad reflectance of light is attributed to the smooth surface of flat PCP and the rough surface of wrinkled PCP, respectively. When the OD is tilted to $\theta = 30°$, the $\lambda_{max}$ = 525 nm at $\theta = 3°$ of the flat PCP shifts to the shorter wavelength (Figure 3g). The original green is totally disappeared by further increasing $\theta = 60°$, and the flat PCP now can be observed as the blue reflection color. According to Bragg's law, the 1D photonic crystals of CLC act as a Bragg reflector, and exhibit selective blueshift reflections as the viewing angle increases along the HA.[26] The reflection wavelength of the flat PCP when observed from the side is affected by the average refractive index ($n$), pitch length ($P_0$), and the viewing angle ($\theta$), which can be expressed by the equation: $\lambda_r = n \times P_0 \times \cos\theta$. However, the wrinkled PCP reflects the same red, green, and blue color as the reflection color at $\theta = 3°$ even with an

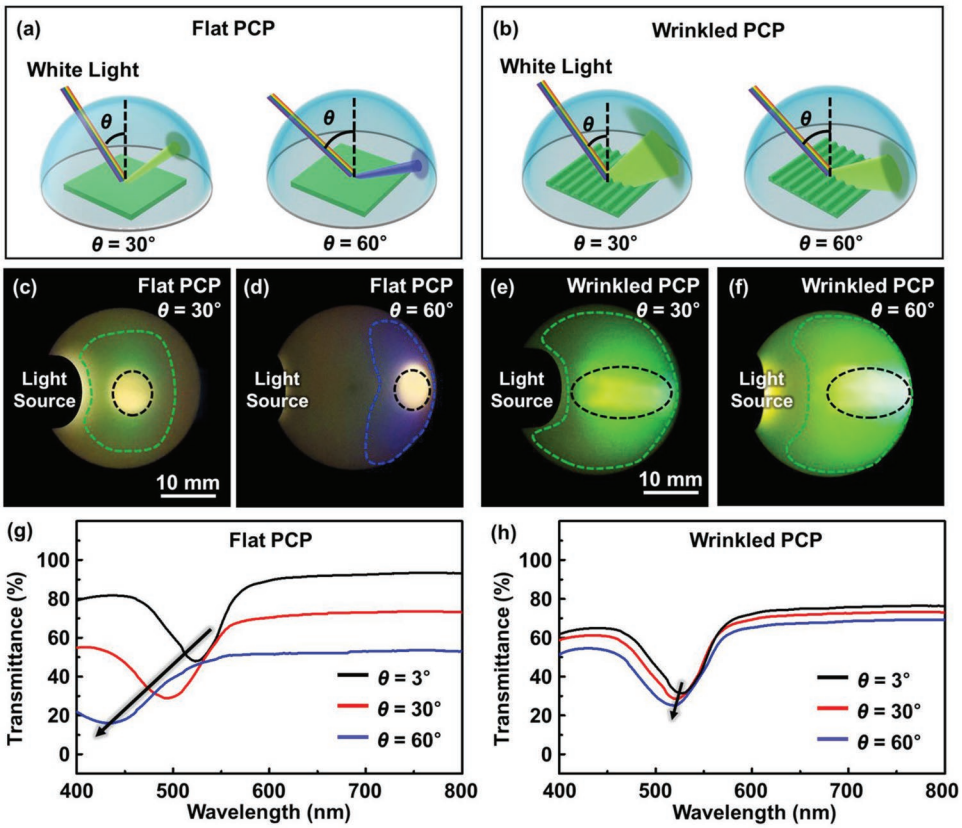


**Figure 3.** Schematic images of the translucent hemispherical dome screen used to visualize the reflection color from a) the flat and b) wrinkled PCP. Top view of reflection color patterns on a dome screen with illumination at c,e) $\theta = 30°$ and d,f) 60°. Transmittance spectra of g) the flat and h) wrinkled PCP.

increased viewing angle over 60°. As shown in Figure 3h, the $\lambda_{max}$ of the notch position is nearly constant for the wrinkled PCP at different $\theta$.

### 2.2. Characterization of Microstructure and Optical Properties of Wrinkled PCP

In contrast to the angular-dependent color reflection of flat PCPs, the wrinkled PCP exhibits angular-independent structural color. Spatial angle dependence of the wrinkled PCP was observed by varying the viewing positions. Here, we introduce the azimuthal rotating angle ($\varphi$) between OD and WD in *ab*-plane and the viewing angle ($\theta$) (**Figure 4**a). The selective reflection of the wrinkled PCP at $\varphi = 0°$ remained constant even though $\theta$ is changed from 3° to 60° (Figure 4b). This result is mainly due to the combination of the micro-scale wrinkled structure and the orientation of the helical nanostructures of the PCP.[27] Because of the axial symmetry of the wrinkled PCP's structure, the Bragg angles are the same around the wrinkle direction, resulting in equal reflections from the film surface along the viewing angle. However, when the film is observed perpendicular to the wrinkle direction, the Bragg angle changes according to the positions of the wrinkles. To visualize the unique helical nanostructures on the wrinkles, their cross-sectional morphology was observed using a scanning electron microscope (SEM). As shown in **Figure 5**a, the distance ($d$) between the crest and its neighboring crest is 118 µm and the height ($A$) between the crest and the valley is $A = 61$ µm.

To further investigate the reasons for the viewing angle independence of wrinkled PCPs, each crest and valley of the wrinkles were magnified and observed. As shown in Figure 5b,c, the cholesteric layers are stacked along the curvature of the crests and valleys, which enables wrinkled PCP to reflect the light at a much wider angle than the flat PCP. The length of the helical pitch ($P_{green}$) is measured to be 340 nm, and this result accords with the selective reflection color of the wrinkled PCP to be green. It is well known that the orientation of the CLC molecule is influenced by the confinement geometry and anchoring condition as a result of the interaction between the CLC molecules and bounding surfaces.[28] Since the CLC molecules are confined within the wrinkles, they are oriented tangentially to the surface and perpendicular to the WD while keeping the helical nanostructure. When the wrinkled PCP is observed at $\theta = 3°$ and $\varphi = 0°$, the reflected color from the cholesteric layer on the highest part of the crest and the lowest part of the valley is most clearly visible, and the same green color as that of the flat PCP is observed. Even on the inclined surface of the wrinkled PCP, the HA is aligned perpendicular to the wrinkled surface. Thus, the same helical pitches can be observed at $\theta = 30°$ and 60°. This unique feature is detected on both the crest and valley slopes, which is responsible for the viewing angle independence of the wrinkled PCP at $\varphi = 0°$. The hierarchical structure of wrinkle PCP is illustrated in Figure 5d.

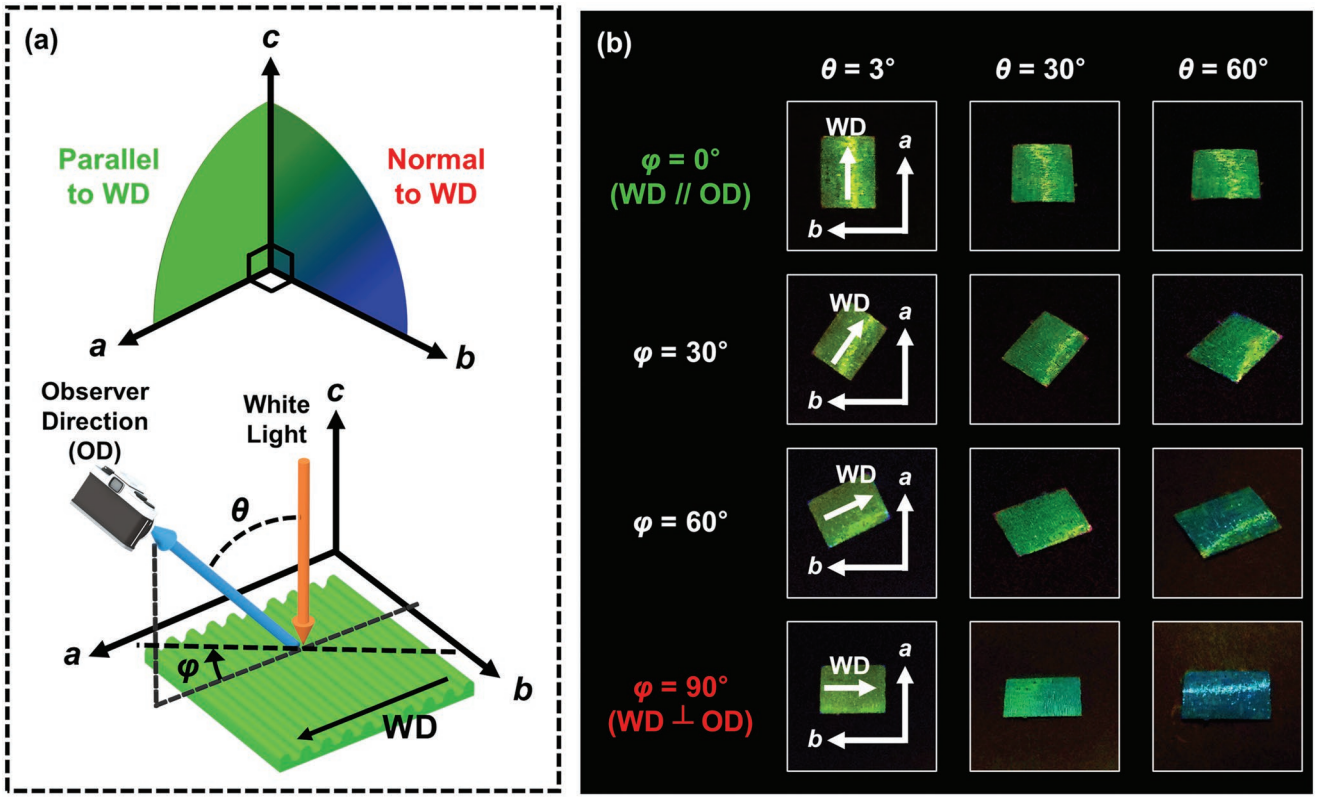


**Figure 4.** a) Schematic illustration of the conditions for observing wrinkled PCP. Here, $\varphi$ is azimuthal rotating angle and $\theta$ is viewing angle. b) Macroscopic image of wrinkled PCP observed by varying the $\theta$ and $\varphi$.

The reflection color change of the wrinkled PCP by altering $\varphi$ further supports that the implantation of the wrinkled morphologies onto the 1D photonic crystals is effective to obtain wide viewing angle. Upon broadening the $\varphi$ (from 0° to 90°) and increasing the $\theta$ (from 3° to 60°), the significant blueshift of reflection color is observed. On the basis of the CIELAB color space, the structural color change to the shorter wavelength region becomes larger as the $\varphi$ approaches to 90° depending on $\theta$ (Figure S5, Supporting Information). The standardized conversion equations are used to convert the red, green, and blue values of each PCP to chromaticity coordinates (Table S1, Supporting Information).[29] By broadening the $\varphi$, the observer is going to stare mainly the helical nanostructures on the tangential plane of the wrinkled morphologies rather than the inclined plane. When the wrinkled PCP is detected at $\varphi = 90°$, it is hard to find the HA along the inclined plane. Therefore, the optical property of wrinkled PCP observed at $\varphi = 90°$ is similar to the flat PCP. This result is originated from the use of uniaxially pre-stretched 1D IPN substrate.

To further control the viewing angle, a wrinkled PCP with different dimensions of the wrinkle morphology was investigated. The angular independence of the wrinkled PCP can be attributed to the HA that is always aligned to reflect toward the observer along the WD.[30] The chiral nematic director is planarly anchored along the wrinkled surface of PCP to maintain a minimal energy state, and HA is oriented perpendicular to the wrinkled surface.[31] The wavelength and amplitude of the wrinkle is programed by applying the pre-stain as 25%, 50%, 100%, 150%, and 200% during the fabrication of the IPN substrate. As shown in Figure S6 (Supporting Information), the wrinkled structure of the IPN substrate is unidirectionally oriented and spontaneously formed with a period of tens to hundreds of micrometers. CLC paints shear-coated on the IPN substrates were photo-polymerized and peeled off to obtain the series of wrinkled PCP having controlled geometries abbreviated as $f_{25}$, $f_{50}$, $f_{100}$, $f_{150}$, and $f_{200}$, respectively (**Figure 6**b). Based on a numerical model (Jones and Berreman method) of light transmission and reflection in the CLC materials, the wrinkled PCP of $f_{25}$, $f_{50}$, $f_{100}$, $f_{150}$, and $f_{200}$ basically reveals the strong metallic lustrous with the selective green light reflection at $\theta = 3°$ because of the sufficient thickness over 100 µm.[32]

The applied force used in the pre-strain process increases the $A/d$ of the wrinkled PCP. The increased $A/d$ can enhance the viewing angle under the given condition. We can always find the selective reflection color determined by the helical pitch of the nanostructure when the OD is parallel to the HA. Here, the angle between the HA and the film thickness direction of the PCP ($z$-axis) is defined as $\delta$ (Figure 6a). For the flat PCP, the viewable angle ($\Delta\delta = \delta_{max} - \delta_{min}$) is very small, because $\delta_{max}$ and $\delta_{min}$ is close to zero according to the Bragg's law, resulting the dramatic color change depending on the $\theta$. Due to the inclined arrangement of the HA along the slope between the crest and the valley, $\delta$ is widely broaden. Since the $\delta_{max}$ can be calculated as $\arctan(2\pi A/d)$, the $\Delta\delta$ of the wrinkled PCP compared to that of the flat PCP is increased along the $\theta$. As shown in Figure 6c, the reflection color of $f_{25}$ and $f_{200}$ is different at $\theta = 60°$. The same green structural color of $f_{200}$ is observed when the $\theta$ is increased up to 60°. Unlike $f_{200}$, the structural color of $f_{25}$ is blue-shifted at $\theta = 60°$ (Figure S7, Supporting Information).

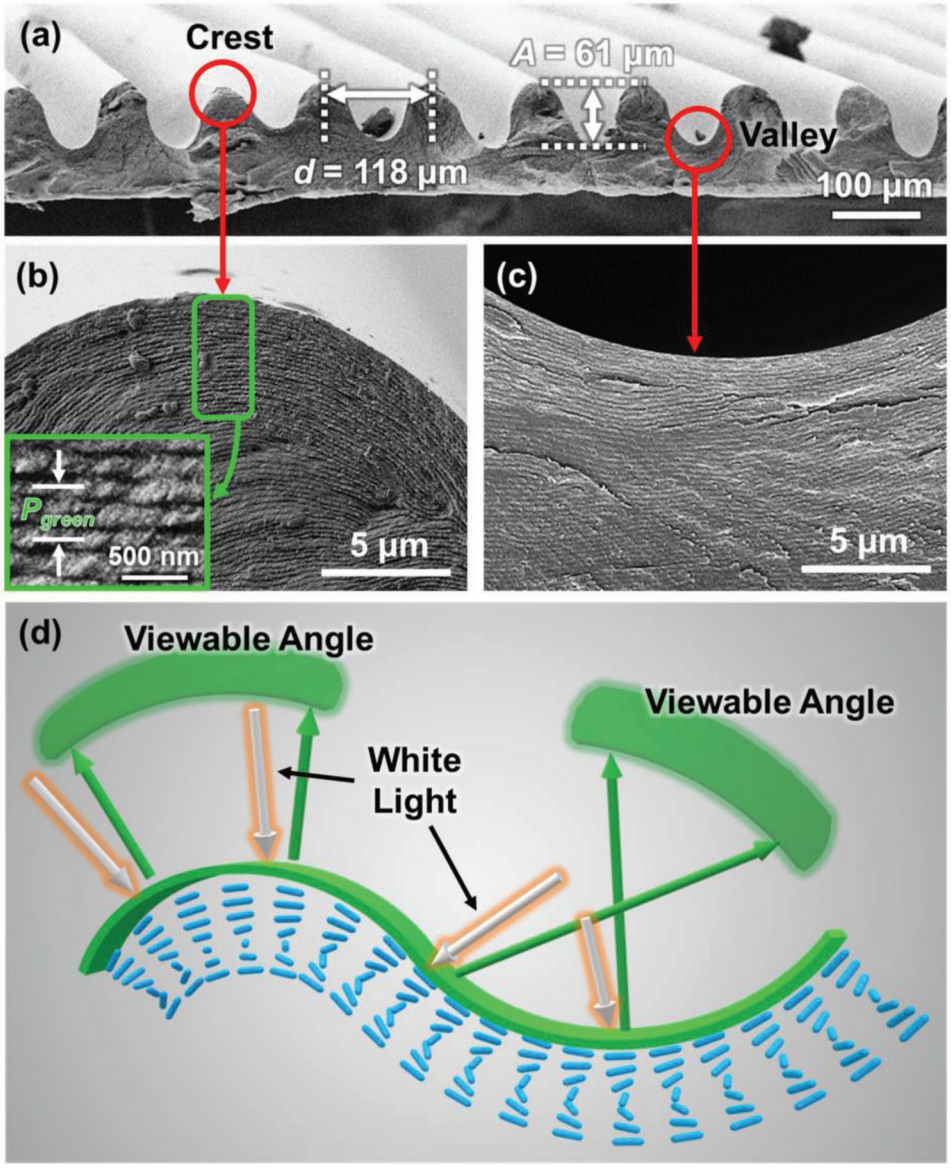


**Figure 5.** a) Cross-sectional SEM image of 1D stripe-wrinkled PCP and observed by magnifying b) the crest and c) the valley. d) Schematic illustration of reflection pathway of the 1D stripe-wrinkled PCP.

Similar to $f_{200}$, $f_{100}$ still shows the green color at $\theta = 60°$, while the $\lambda_{max}$ of the notch position shifts to the short wavelength region at $\theta = 80°$. The calculated viewable angle of $\Delta\delta$ derived from the real dimension of $A/d$ with the $f_{25}$, $f_{100}$, and $f_{200}$ is 50.3°, 73.3°, and 75.1°, respectively. The manipulation of $A/d$ by simple stretching and releasing process can easily control the broadening of structural color cues (Figure 6d).

### 2.3. 2D Wrinkle Structure for Viewing Angle Independency in All Directions

Based on our understanding of the relationship between the wrinkled structures and reflection notches, the wrinkled PCP is applied as a patternable 2D PCP. The viewing angle independence of 1D stripe-wrinkled PCP varies according to the viewing direction. Thus, we can fabricate a film that reflects different patterns depending on the observation direction by arranging the wrinkle directions of different patterns orthogonal to each other (**Figure 7**a). First, a butterfly-shaped hole is cut into the uniaxially wrinkled IPN substrate. As in a jigsaw puzzle, an IPN substrate with orthogonal wrinkle patterns can be fabricated by filling the holes with a butterfly-shaped substrate with wrinkles perpendicular to the base substrate. The CLC mixture that reflected green color was shear-coated on the 2D patterned IPN substrate and then photo-polymerized with UV light. As expected, the polymerized film reflects green color uniformly over the entire area when viewed from the front (Figure 7b). As illustrated in Figure 7c, by observing the boundary line of the orthogonal pattern in the reflection mode of an optical

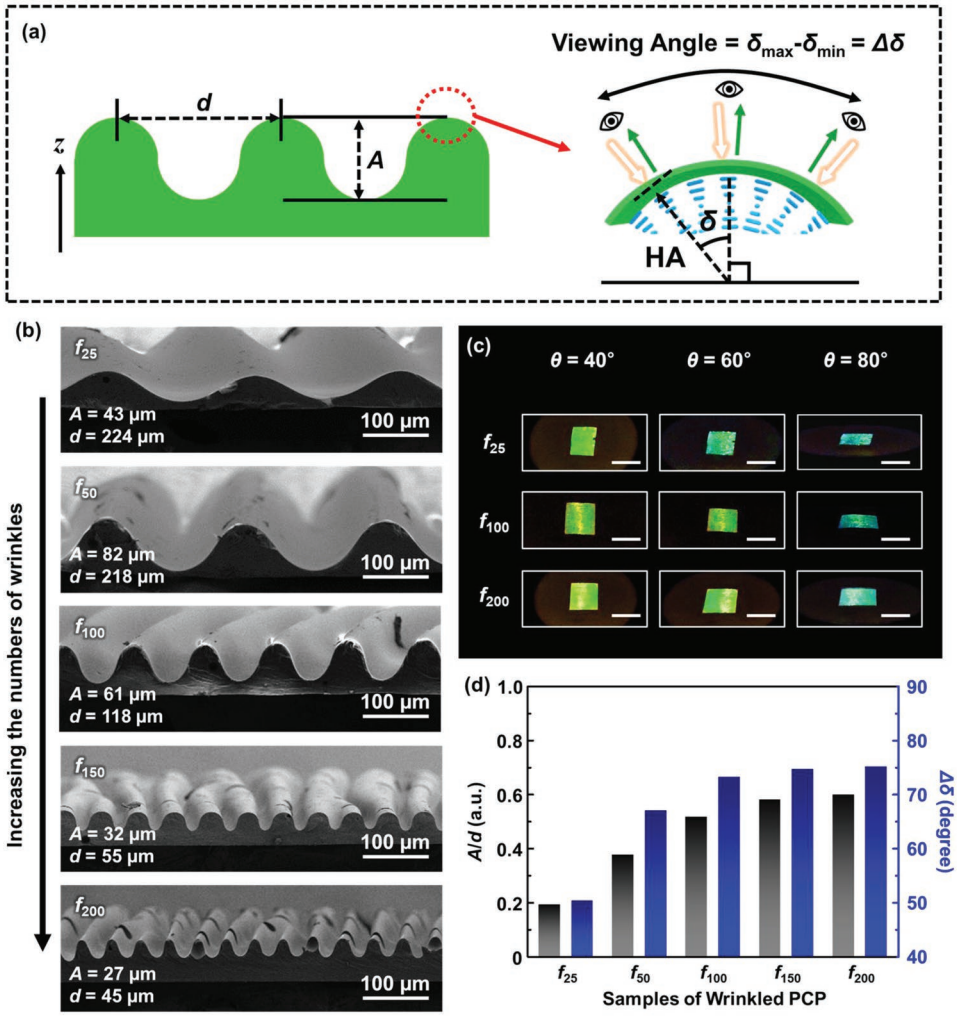


**Figure 6.** a) Schematic illustration for wrinkled geometry of PCP and its viewing angles. b) Cross-sectional SEM images of the wrinkled PCP with controlled $A/d$. c) Macroscopic images of $f_{25}$, $f_{100}$, and $f_{200}$ observed at $\theta = 40°$, 60°, and 80°. The scale bar in the image is 10 mm. d) $A/d$ and $\Delta\delta$ of the wrinkled PCPs.

microscope, it was confirmed that the spacing of each intersecting wrinkle is the same. When the film with the butterfly pattern is viewed from the side, the reflection color changes depending on the direction of observation as the viewing angle of the 1D stripe-wrinkled PCP varies depending on the direction of the wrinkles. Figure 7d,e shows a schematic illustration of the observation of the 2D-wrinkled PCP and an actual image. When observed from the direction parallel to the wrinkles on the butterfly pattern, the butterfly pattern maintains the green color reflected wavelength due to the morphology of the wrinkles. However, the background is not visible because it is outside of the viewing angle. Rotating the film 90° darkens the butterfly pattern and the strong green reflection is observed in the background.

By uniaxially stretching the base AR/SR, regular repetitive waves can be produced during the 1D stripe-wrinkled PCP fabrication process. To demonstrate the fabrication of complex wrinkled PCP in a single process, a biaxially stretched IPN substrate was fabricated. The base AR/SR was stretched by 50%, simultaneously in the *x*-axis and *y*-axis direction, and then cured at 100 °C for 1 h. As shown in **Figure 8**a, the biaxially stretched IPN substrate has a more complex pattern than the uniaxially stretched IPN substrate, evidenced by a sinuous wavy wrinkle pattern on the plane surface, which forms in order to minimize the elastic energy applied to the substrate.[33] Similarly, in the case of a 2D wavy pattern, the topology of the substrate can be transferred to PCP by shear coating the CLC mixture (Figure 8b). Unlike the 1D stripe-wrinkled PCP, the PCP with a 2D wavy pattern has crests and valleys in all directions. Therefore, it reflects the same green wavelength in all directions. As shown in Figure 8c, the 2D wavy-wrinkled PCP has a matte surface compared to the shiny flat PCP. This matte appearance is due to the fact that, regardless of viewing angle, chiral nematic domains are always positioned favorably to reflect toward the observer, giving the film's coloring more angular independence under diffuse illumination. The diffusive character of the scattering response of the film is observed in different directions, including those orthogonal to each other. The 2D wavy-wrinkled PCPs reflect the same green color when viewed from all directions (direction (i) and (ii)). To investigate the angular independence of the wrinkled PCP, the wavelength distribution of the maximum reflection peak of the flat and wrinkled

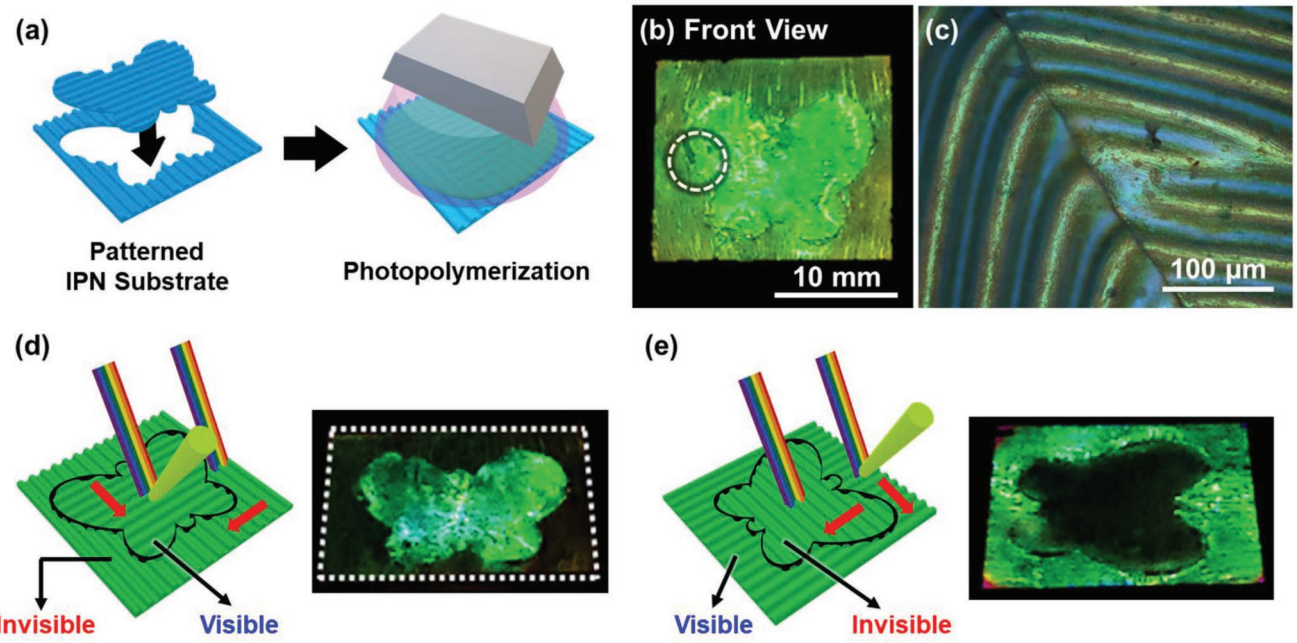


**Figure 7.** a) Fabrication process of the patterned and wrinkled PCP. b) Macroscopic image of the patterned and wrinkled PCP observed from the front and c) OM image of the pattern boundary in reflection mode. Macroscopic images and corresponding schematic illustrations when observed d) parallel and e) perpendicular to the wrinkle direction on the butterfly pattern.

PCP was measured at various viewing angles (Figure 8d). Both the flat and the wrinkled PCP exhibit maximum reflection at 540 nm when observed from the front ($\theta = 0°$), and reflect the green color. At a viewing angle of 70°, the maximum reflection wavelength of the flat PCP was shifted to a shorter wavelength ($\lambda_{max} = 430$ nm), but the maximum reflection wavelength of the wavy-wrinkled PCP maintains a similar green color ($\lambda_{max} = 528$ nm).

## 3. Conclusion

1D stripe and 2D wavy wrinkled photonic crystal paper (PCP) was developed to demonstrate directional independent reflection colors by corrugating PCPs with 1D helical nanostructures. A reactive CLC mixture was shear-coated on the 1D and 2D wrinkled interpenetrating polymer network (IPN) rubber

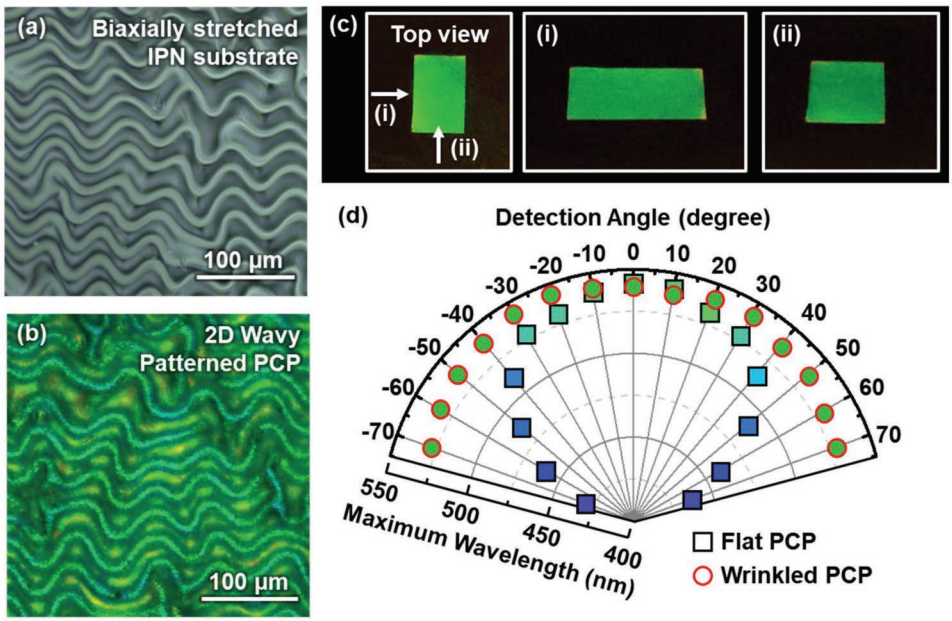


**Figure 8.** a) OM image of the biaxially stretched IPN substrate and b) the 2D wavy patterned PCP. c) Macroscopic image of 2D wavy patterned CLC film observed from the front, and transverse, and longitudinal sides. d) Maximum wavelength distribution of the reflection peak for the flat PCP and wrinkled PCP, at different viewing angles.

substrate and stabilized by photo-polymerization. POM and SEM observations confirmed the formation of micrometer-scale wrinkles on the surface of the PCP, as well as the formation of helical nanostructures in the cross section along the grooves. When the flat PCP was observed at a viewing angle of 60°, the reflection wavelength was blueshifted by 95 nm; however, the reflected wavelength of the wrinkled PCP remained nearly constant even when the viewing angle was increased. Since the 1D stripe-wrinkled PCP affects the anisotropic angular dependence of the CLC film, it is possible to modify the pattern direction on the IPN substrate to produce an anti-counterfeiting film that reflects different patterns depending on the viewing direction. 2D wavy-wrinkled PCP reflects the same color regardless of the viewing angle direction and can be used to fabricate monochromatic light reflectors with wide viewing angles.

## 4. Experimental Section

*Materials*: Chiral RM (BPcRM) with a helical twisting power of 22 $\mu m^{-1}$ was synthesized according to a previously reported method.[20] Achiral RM (RM257 and LC242), acrylic rubber (VHB-4910, 3M ), silicone rubber (Sylgard-184 kit, Dow Corning), and *n*-heptane were purchased and used without further purification. 2,2-Dimetoxy-2-phenylacetophenone (Irgacure 651) was used as a 365 nm UV light photoinitiator.

*Fabrication of 1D and 2D Wrinkled IPN Substrate*: A Sylgard-184 kit consists of two parts: one is a dimethyl vinyl-terminated silicone-based polymer (Sylgard A), and the other one is a cross-linker with a platinum-based catalyst (Sylgard B). Sylgard A, Sylgard B, and *n*-heptane solvent were mixed in a weight ratio of 10:1:10 to form a Sylgard 184 solution. Acrylic rubber film was then immersed into the Sylgard 184 solution. After equilibrium swelling, the SR wrapped swollen AR was dried at room temperature for 2 h to remove the solvent. The AR/SR substrate was pre-strained in uniaxial and biaxial directions. The pre-strained AR/SR substrate was then placed in an air oven at 100 °C for 1 h in order to fully cure the guest SR molecules. After curing, the AR/SR substrate exhibited sinusoidal stripe wrinkles and 2D wave-like wrinkles on its surface, in the direction of the pre-strain.

*Macroscopic Imaging of Reflection Color*: Flat and wrinkled PCP was placed on a piece of black paper. For selected area illumination, a white LED light (Thorlabs, MWWHF2) equipped with a 400 µm diameter fiber optic cable and collimating lens (CFC-2X-A) was used. A translucent hemisphere dome was created by cutting a white ping pong ball in half and drilling a 3 mm diameter hole in the side, in order to capture the reflected color pattern. The ping pong ball dome screen was then placed on the PCP and collimated light from the LED passed through the hole.

*Characterization*: The reflective light of the photonic crystal paper was measured by UV–vis spectroscopy (SCINCO-3100). The optical textures of the CLC phases were imaged using polarized optical microscopy (Nikon Eclipse E600) with transmission and reflection modes. The cross-sectional image of the photonic crystal paper was obtained using field-emission scanning electron microscopy (FE-SEM, Carl Zeiss, SUPRA 40VP). For SEM observation, the wrinkled PCP was frozen in liquid nitrogen for 5 min and then rapidly cut with a razor blade.

## Supporting Information

Supporting Information is available from the Wiley Online Library or from the author.

## Acknowledgements

This work was supported by Basic Research Laboratory Program (2020R1A4A1018259), Mid-Career Researcher Program (2021R1A2C2009423), and Korea Government MSIT (2021R1R1R1004226).

## Conflict of Interest

The authors declare no conflict of interest.

## Data Availability Statement

The data that support the findings of this study are available from the corresponding author upon reasonable request.

## Keywords

angle independence, cholesteric liquid crystals, interpenetrating polymer networks, photonic crystal papers, wrinkle structures

Received: July 25, 2022
Revised: September 29, 2022
Published online: November 27, 2022

[1] M. Mitov, *Adv. Mater.* **2012**, *24*, 6260.
[2] C. Binet, M. Mitov, A. Boudet, *Mol. Cryst. Liq. Cryst. Sci. Technol. Sect. A-Mol. Cryst. Liq. Cryst.* **2000**, *339*, 111.
[3] A. Matranga, S. Baig, J. Boland, C. Newton, T. Taphouse, G. Wells, S. Kitson, *Adv. Mater.* **2013**, *25*, 520.
[4] a) M. Mitov, *Soft Matter* **2017**, *13*, 4176; b) L. Wang, A. M. Urbas, Q. Li, *Adv. Mater.* **2020**, *32*, 1801335; c) H. Zhou, J. Xu, X. Liu, H. Zhang, D. Wang, Z. Chen, D. Zhang, T. Fan, *Adv. Funct. Mater.* **2018**, *28*, 1705309.
[5] a) S. Cormier, T. Ding, V. Turek, J. J. Baumberg, *Adv. Opt. Mater.* **2018**, *6*, 1800208; b) T. Ding, C. Rüttiger, X. Zheng, F. Benz, H. Ohadi, G. A. Vandenbosch, V. V. Moshchalkov, M. Gallei, J. J. Baumberg, *Adv. Opt. Mater.* **2016**, *4*, 877; c) X. Duan, N. Liu, *ACS Nano* **2018**, *12*, 8817; d) H. Lee, T. Y. Jeon, S. Y. Lee, S. Y. Lee, S. H. Kim, *Adv. Funct. Mater.* **2018**, *28*, 1706664; e) C. Liu, G. Wang, L. Zhang, F. Fan, X. Zhang, Y. Fu, T. Wang, *ACS Appl. Mater. Interfaces* **2022**, *14*, 7200.
[6] a) W. Hong, Z. Yuan, X. Chen, *Small* **2020**, *16*, 1907626; b) C. Yang, B. Wu, J. Ruan, P. Zhao, L. Chen, D. Chen, F. Ye, *Adv. Mater.* **2021**, *33*, 2006361; c) Y. Yang, D. Zhou, X. Liu, Y. Liu, S. Liu, P. Miao, Y. Shi, W. Sun, *Opt. Express* **2020**, *28*, 31872; d) W. Yao, R. Lan, K. Li, L. Zhang, *ACS Appl. Mater. Interfaces* **2021**, *13*, 1424.
[7] C. Liu, Y. Long, B. Yang, G. Yang, C.-H. Tung, K. Song, *Sci. Bull.* **2017**, *62*, 938.
[8] a) A. G. Dumanli, T. Savin, *Chem. Soc. Rev.* **2016**, *45*, 6698; b) S. Kinoshita, S. Yoshioka, J. Miyazaki, *Rep. Prog. Phys.* **2008**, *71*, 076401.
[9] Y. Takeoka, *J. Mater. Chem.* **2012**, *22*, 23299.
[10] R. O. Prum, R. H. Torres, *J. Exp. Biol.* **2004**, *207*, 2157.
[11] R. O. Prum, J. A. Cole, R. H. Torres, *J. Exp. Biol.* **2004**, *207*, 3999.
[12] a) S. Schauer, M. Worgull, H. Hölscher, *Soft Matter* **2017**, *13*, 4328; b) S. Vignolini, E. Moyroud, B. J. Glover, U. Steiner, *J. R. Soc. Interface* **2013**, *10*, 20130394.
[13] a) J. Won, S. Mondal, J. Park, W. Wang, H. Lee, S. Kim, B. Shin, S. G. Sathi, C. Nah, *Polym. Compos.* **2020**, *41*, 2210; b) K. Wu, T. Zhu, L. Zhu, Y. Sun, K. Chen, J. Chen, H. Yuan, Y. Wang, J. Zhang, G. Liu, *Nano Lett.* **2022**, *22*, 2261.
[14] a) C. M. Chen, S. Yang, *Polym. Int.* **2012**, *61*, 1041; b) G.-B. Lee, S. G. Sathi, D.-Y. Kim, K.-U. Jeong, C. Nah, *Polym. Test.* **2016**, *53*, 329; c) M. Watanabe, *Soft Matter* **2012**, *8*, 1563; d) Y. Wei, T. Kshetri, P. Bhuyan, C. Nah, S. Park, *Compos. Pt. B: Eng.* **2020**, *190*, 107929.
[15] a) R. Huang, Z. Suo, *J. Appl. Phys.* **2002**, *91*, 1135; b) T. Ohzono, M. Shimomura, *Phys. Rev. B* **2004**, *69*, 132202.

[16] a) P. Kim, Y. Hu, J. Alvarenga, M. Kolle, Z. Suo, J. Aizenberg, *Adv. Opt. Mater.* **2013**, *1*, 381; b) S. M. Mahpeykar, Q. Xiong, J. Wei, L. Meng, B. K. Russell, P. Hermansen, A. V. Singhal, X. Wang, *Adv. Opt. Mater.* **2016**, *4*, 1106; c) S. Schauer, R. Schmager, R. Hünig, K. Ding, U. W. Paetzold, U. Lemmer, M. Worgull, H. Hölscher, G. Gomard, *Opt. Mater. Express* **2018**, *8*, 184.
[17] X. A. Zhang, Y. Jiang, R. B. Venkatesh, J. R. Raney, K. J. Stebe, S. Yang, D. Lee, *ACS Appl. Mater. Interfaces* **2020**, *12*, 7658.
[18] X. Gao, J. Li, T. Li, Z. Su, X. Ma, J. Yin, X. Jiang, *Adv. Funct. Mater.* **2021**, *31*, 2106754.
[19] a) A. Chiche, C. M. Stafford, J. T. Cabral, *Soft Matter* **2008**, *4*, 2360; b) G. Chu, A. Camposeo, R. Vilensky, G. Vasilyev, P. Martin, D. Pisignano, E. Zussman, *Matter* **2019**, *1*, 988.
[20] D.-Y. Kim, C. Nah, S.-W. Kang, S. H. Lee, K. M. Lee, T. J. White, K.-U. Jeong, *ACS Nano* **2016**, *10*, 9570.
[21] a) S. Javadian, N. Dalir, A. G. Gilani, J. Kakemam, A. Yousefi, *J. Chem. Thermodyn.* **2015**, *80*, 22; b) M. Okumuş, *J. Therm. Anal. Calorim.* **2015**, *120*, 1603.
[22] a) G. C. Ingavle, N. H. Dormer, S. H. Gehrke, M. S. Detamore, *J. Mater. Sci.: Mater. Med.* **2012**, *23*, 157; b) C. Marykutty, G. Mathew, S. Thomas, *Rubber Chem. Technol.* **2007**, *80*, 809; c) S. M. Ha, W. Yuan, Q. Pei, R. Pelrine, S. Stanford, *Adv. Mater.* **2006**, *18*, 887; d) G. Kickelbick, *Prog. Polym. Sci.* **2003**, *28*, 83.
[23] I. Dierking, *Textures of Liquid Crystals*, John Wiley & Sons, New Jersey, USA **2003**.
[24] W. J. Yoon, Y. J. Choi, S. I. Lim, J. Koo, S. Yang, D. Jung, S. W. Kang, K. U. Jeong, *Adv. Funct. Mater.* **2020**, *30*, 1906780.
[25] a) A. E. Goodling, S. Nagelberg, B. Kaehr, C. H. Meredith, S. I. Cheon, A. P. Saunders, M. Kolle, L. D. Zarzar, *Nature* **2019**, *566*, 523; b) S. Y. Lee, J. Yoon, S.-H. Kim, *Chem. Mater.* **2021**, *33*, 4628.
[26] M. Schwartz, Y. Geng, H. Agha, R. Kizhakidathazhath, D. Liu, G. Lenzini, J. P. Lagerwall, *Multifunct. Mater.* **2021**, *4*, 022002.
[27] H. Gu, Y. Zhao, Y. Cheng, Z. Xie, F. Rong, J. Li, B. Wang, D. Fu, Z. Gu, *Small* **2013**, *9*, 2266.
[28] H.-Q. Chen, X.-Y. Wang, H. K. Bisoyi, L.-J. Chen, Q. Li, *Langmuir* **2021**, *37*, 3789.
[29] a) P. Lin, Y. Cong, C. Sun, B. Zhang, *Nanoscale* **2016**, *8*, 2403; b) W. Lv, Y. Jia, Q. Zhao, M. Jiao, B. Shao, W. Lü, H. You, *Adv. Opt. Mater.* **2014**, *2*, 183; c) C. Luo, B. Yao, Y. Lu, C. Huang, Z. Wang, X. Du, J. Zhou, A. Reheman, J. Wang, *Macromol. Mater. Eng.* **2022**, *307*, 2100594.
[30] C. L. C. Chan, M. M. Bay, G. Jacucci, R. Vadrucci, C. A. Williams, G. T. van de Kerkhof, R. M. Parker, K. Vynck, B. Frka-Petesic, S. Vignolini, *Adv. Mater.* **2019**, *31*, 1905151.
[31] P. Rofouie, D. Pasini, A. Rey, *J. Chem. Phys.* **2015**, *143*, 114701.
[32] D.-Y. Kim, K. M. Lee, T. J. White, K.-U. Jeong, *NPG Asia Mater.* **2018**, *10*, 1061.
[33] L. Pellegrino, S. Khodaparast, J. T. Cabral, *Soft Matter* **2020**, *16*, 595.